Arabian Journal for Science and Engineering (2023) 48:7411–7424
https://doi.org/10.1007/s13369-022-07477-y

RESEARCH ARTICLE-CHEMISTRY

Biosynthesis and Analytical Characterization of Iron Oxide Nanobiocomposite for In-Depth Adsorption Strategy for the Removal of Toxic Metals from Drinking Water

Ashfaque Ali Bhutto[1] · Jameel Ahmed Baig[1] · Sirajuddin[2] · Tasneem Gul Kazi[1] · Reyes Sierra-Alvarez[3] · Khalil Akhtar[1] · Sajjad Hussain[4] · Hassan Imran Afridi[1] · Aysen Hol[5] · Suraya Samejo[1,5]

Received: 31 August 2022 / Accepted: 9 November 2022 / Published online: 23 November 2022

Abstract

The biosynthesis of the iron oxide nanoparticles was done using *Ixoro coccinea* leaf extract, followed by the fabrication of iron oxide nanobiocomposites (I-Fe_3O_4-NBC) using chitosan biopolymer. Furthermore, the synthesized I-Fe_3O_4-NPs and I-Fe_3O_4-NBC were characterized, and I-Fe_3O_4-NBC was applied to remove toxic metals (TMs: Cd, Ni, and Pb) from water. The characterization study confirmed that the nanostructure, porous, rough, crystalline structure, and different functional groups of chitosan and I-Fe_3O_4-NPs in I-Fe_3O_4-NBCs showed their feasibility for the application as excellent adsorbents for quantitative removal of TMs. The batch mode strategy as feasibility testing was done to optimize different adsorption parameters (pH, concentrations of TMs, dose of I-Fe_3O_4-NBC, contact time, and temperature) for maximum removal of TMs from water by Fe_3O_4-NBC. The maximum adsorption capacities using nanocomposites for Cd, Ni, and Pb were 66.0, 60.0, and 66.4 mg g^{-1}, respectively. The adsorption process follows the Freundlich isotherm model by I-Fe_3O_4-NBC to remove Cd and Ni, while the Pb may be adsorption followed by multilayer surface coverage. The proposed adsorption process was best fitted to follow pseudo-second-order kinetics and showed an exothermic, favorable, and spontaneous nature. In addition, the I-Fe_3O_4-NBC was applied to adsorption TMs from surface water (%recovery > 95%). Thus, it can be concluded that the proposed nanocomposite is most efficient in removing TMs from drinking water up to recommended permissible limit.

Keywords I-Fe_3O_4-NPs · I-Fe_3O_4-NBC · Adsorption · Toxic metals · Kinetics · Thermodynamics · Surface water

1 Introduction

The quality of drinking water resources is continuously contaminated due to undesirable constituents [1]. The drinking water can be contaminated by industrialization, domestic and agricultural activities, and other environmental/global changes [2, 3]. Polluted water may contain several contaminants, especially toxic metals (TMs: Cd, Ni, and Pb).

✉ Jameel Ahmed Baig
jameel.baig@usindh.edu.pk

Sirajuddin
drsiraj03@yahoo.com

Tasneem Gul Kazi
tasneem.kazi@usindh.edu.pk

Reyes Sierra-Alvarez
rsierra@arizona.edu

Sajjad Hussain
sajjad.phd.cssp@pu.edu.pk

Hassan Imran Afridi
hassan.afridi@usindh.edu.pk

Aysen Hol
aozdag@pau.edu.tr

Suraya Samejo
suraya.samejo@scholars.usindh.edu.pk

1 Centre of Excellence in Analytical Chemistry, University of Sindh, Jamshoro 76080, Pakistan

2 ICCBS, HEJ, University of Karachi, Karachi 75270, Pakistan

3 Department of Chemical and Environmental Engineering, University of Arizona, Tucson, AZ 85721-0011, USA

4 Centre of Excellence in Solid State Physics, University of the Punjab, Lahore 05422, Pakistan

5 Chemistry Department, Pamukkale University, 20017 Denizli, Turkey

These TMs are among the main inorganic pollutants produced by the electroplating, steel, and battery industries [4]. Moreover, these TMs may also remain in our surroundings for a longer time and leach into underground water and soil/land when in contact with them. It may lead to a potential threat to livings beings [5]. Purifying contaminated water (industrial, agricultural, and domestic wastewater) is the best strategy to reduce water pollution before discharging it into the environment [6]. Subsequently, these TMs bioaccumulate in the plants and enter the food chain. These TMs can cause various severe dysfunctions and cancer [7, 8]. The best management of polluted water is to purify the contaminated/polluted water before reuse/drain/escape. Various strategies have been employed to filter polluted water for decades, like membrane filtration [9], reverse osmosis [10], chemical precipitation [11], ion exchange [12], and adsorption [13]. Among these strategies, adsorption is the most efficient, attractive, economical, and practical purification strategy [14]. The adsorption process using different materials (adsorbents) is the most prominent treatment strategy based on its low cost and ease of operation [15, 16]. Natural adsorbents like zeolites, mesoporous silica, activated porous carbon, rice husk, and wood sawdust are used. Synthetic adsorbents such as alumina [17], zinc oxide [17], titanium dioxide [17], iron oxide nanoparticles [18], and other nanomaterials have been adopted for achieving the promising potential for environmental cleanup [14, 19].

Iron oxide nanoparticles (FeO-NPs) are attractive adsorbents for the TMs removal from contaminated drinking water [20]. It is because of their essential features like small size, high surface area, magnetic property, and reusability [21]. Moreover, FeO-NPs have significant variable oxidation states, crystal structures, low cost, magnetic properties, and environment-friendly nature [22]. Generally, FeO-NPs are synthesized using reactive and toxic reducing agents, i.e., sodium borohydride and hydrazine hydrate, which may cause undesired detrimental impacts on the environment, plants, animals, and human beings. Thus, it is a need of hours to develop facile, effective, and green chemical processes for their production [23]. Based on these facts, various microorganisms (actinomycetes, bacteria, fungi, algae, and viruses) were used to produce stable and well-functionalized iron oxide nanoparticles as clean, eco-friendly, and sustainable precursors [24]. The cost of iron oxide nanoparticle production for consumers and industries must maintain a delicate balance between environmentally sound green processes and their sustainability. Thus, it is vitally important to explore a more reliable and sustainable process for synthesizing FeO-NPs.

The synthesis of iron oxide nanoparticles using plant-derived chemicals is the most cost-effective. Plant extracts may include compounds that function as reducing and capping agents, such as organic acids, proteins, amino acids, polysaccharides, terpenoids, aldehydes, ketones, and amides. These are reported for the size-controlled synthesis of nanoparticles [25, 26]. For example, the synthesis of Fe and Fe oxide NPs using extracts of different plants (e.g., *Caricaya papaya*, *Azadirachta indica*, *Carob* leaves, *Ficus carica*, *Phyllanthus niruri*, *Platanus orientalis*, and *Citrus medica*) [27–33] has been described and developed a facile method to fabricate metal oxide nanoparticles of different morphologies [34]. The green method can synthesize iron oxide nanoparticles by co-precipitation methods, which can then be used to remove TMs from aqueous solutions. This method does not require an organic solvent for the prevention of agglomeration to produce nanoparticles with an average diameter size of 50 nm [35]. This approach provides advantages over chemical and physical methods as it is cost-effective, environment-friendly, and easily scaled up for large-scale synthesis with no need to use high pressure, energy, temperature, or toxic chemicals [31]. Therefore, for the current study, the Jungle geranium (*Ixora coccinea*) was first time selected based on the presence of several organic lupeol, oleanolic acid, ursolic acid, sitosterol, lecocyanadin, rutin, proanthocyanidins, anthocyanins, quercetin, and glycosides of kaempferol [36].

Various polymeric materials are used to fabricate iron oxide nanocomposites, including polyvinyl alcohol, chitosan, polyurethane, barium titanate, vinyl ester resin, alginate, and gum [37–40]. Moreover, natural biopolymers, especially chitosan, can be utilized to synthesize nanocomposite (NBC) [41]. Chitosan is a biopolymer (polysaccharide). It has stable, non-toxic chemical and suitable adhesive properties, which makes it highly reactive. It is readily soluble in acidic solution and is not used as an adsorbent for wastewater treatment because of these distinct disadvantages [42]. To address the major drawbacks and to investigate the great adsorbability of chitosan, its adsorption efficiencies can be essentially improved when it can be modified by grafting [43], cross-linking [44], and functionalization [45] to form new composites. The chitosan has a high proportion of amine groups ($–NH_2$) and hydroxyl groups (–OH), which provide active sites for the fabrication of nanocomposites with metal/metal oxide [46]. Recent studies showed that nanobiocomposites (NBCs) are promising to remove TMs and other contaminants [47, 48]. The iron oxide NBC coated with natural biopolymeric material showed excellent removal of TMs because of the high surface area, porous structure, and active sites ($–NH_2$/–OH) on the surface of nanostructures [49]. Moreover, these magnetic nanomaterials are recyclable, low cost, and can be easily manipulated by an external magnetic field [49].

The current study is designed to synthesize the magnetic iron oxide nanoparticles (I-Fe_3O_4-NPs) using *Ixora coccinea* leaf extract. These biosynthesized I-Fe_3O_4-NPs were coated with chitosan to obtain iron oxide NBC (I-Fe_3O_4-NBC).

The characterizations of I-Fe_3O_4-NPs and I-Fe_3O_4-NBC were conducted by X-ray diffraction (XRD), atomic force microscope (AFM), Fourier transform infrared spectroscopy (FT-IR), scanning electron microscopy (SEM), UV–visible spectroscopy, and dynamic light scattering (DLS). After that, the I-Fe3O4-NBC was successfully applied to remove TMs from the aqueous solution. The experimental parameters (i.e., pH, adsorbent dose, contact time, analyte concentration, and temperature), adsorption behavior, and reaction kinetics were studied in detail.

2 Materials and Methods

2.1 Materials

All the chemicals and reagents were of high purity analytical grade. Ferric chloride ($FeCl_3{\cdot}6H_2O$), hydrochloric acid (HCl 37%), sodium hydroxide (NaOH), and chitosan ($C_{56}H_{103}N_9O_{39}$) were purchased from Sigma-Aldrich (Louis, USA). Ferrous sulfate ($Fe_2SO_4{\cdot}7H_2O$), cadmium chloride ($CdCl_2{\cdot}H_2O$), nickel nitrate ($Ni(NO_3)_2{\cdot}6H_2O$), acetic acid ($C_2H_4O_2$), and sodium acetate (CH_3COONa) were purchased from MERCK (Darmstadt, Germany). The certified standard stock solutions of Cd, Ni, and Pb (1000 mg L^{-1}) were purchased from Sigma-Aldrich. The working standards are prepared from stock solutions by successive dilution. The deionized water obtained from a water purifier (Bedford, USA) and pH meter (Eutech, Malaysia) were used.

2.2 Collection and Preparation of *Ixora coccinea* Plant Leaf Extract

The scientific protocol proposed by Iravani et al. [50] was adopted to choose promising indigenous plants for NPs synthesis. The plants are capable of heavy metal accumulation and detoxification [50] and contain natural reducing and stabilizing agents [25, 26, 50]. Leaves of jungle geranium (*Ixora coccinea*) were collected from the NCEAC garden of the University of Sindh, Jamshoro. The plant may have amino, carboxyl, and hydroxyl functionalities containing phytochemicals. The active functionality of phytochemicals can act as active metal reducing and capping agents for synthesizing sustainable metal oxide nanoparticles [51]. The synthesis of *Ixora coccinea* leaf extract-based-iron oxide nanoparticles (I-Fe_3O_4-NPs) was successfully achieved.

The fresh leaves of *Ixora coccinea* were washed multiple times with tap water, followed by DIW to remove the dust particles. The leaves were dried in an electric oven for half an hour at a temperature of 70 °C and cut into small pieces using a sterilized knife. Then 20.0 g of leaves was taken into a 250-mL conical flask and 100.0 mL of DIW. Then, the conical flask was placed on the electric hot plate at 80.0 °C for two hours. Then, the prepared *Ixora coccinea* leaf extract was filtered by Whatman filter paper and stored at 4.0 °C until further experiments.

2.3 Biosynthesis of Iron Oxide Nanoparticles (I-Fe_3O_4-NPs)

The synthesis of I-Fe_3O_4-NPs was carried out by a simple and cost-effective co-precipitation method [52]. 200 mL mixture of precursor salt solution of 1 mM $FeCl_3.6H_2O$ and 1 mM Fe_2SO_4. $7H_2O$ (1:1 v/v) was taken in a 500-mL conical flask and heated at 80.0 °C on the electric hot plate. After that, 100 mL of prepared leaf extract of *Ixora coccinea* was added dropwise by conical flask with continuous stirring at 100 rpm. The addition of *Ixora coccinea* leaves to extract the light brown color solution started to change into blackish suspension, indicating the formation of I-Fe_3O_4-NPs. After 2.0 h, the resulting suspension was cooled at room temperature and filtered with Whatman filter paper. The obtained particles were washed by DIW followed by ethanol to remove impurities and dried in an electric oven at 105 °C to get a result of a dark black colored powder. The resulting powder was calcinated in a muffle furnace at 600 °C for 4 h to oxidize the organic compounds, and pure I-Fe_3O_4-NPs were obtained. The resulting I-Fe_3O_4-NPs were characterized by various analytical techniques to study their morphological and structural characteristics.

2.4 Biosynthesis of Iron Oxide Nanobiocomposites (I-Fe_3O_4-NBC)

Iron oxide nanobiocomposites (I-Fe_3O_4-NBC) were synthesized following the reported method elsewhere [52]. The synthesized iron oxide nanoparticles I-Fe_3O_4-NPs were dispersed in 10.0 mL of chitosan (0.5 mg mL^{-1}) in an acetate buffer solution of pH 4.20. The solution was stirred at 100 rpm for 4.0 h on the electric stirring plate at room temperature. After that, the resultant suspension was sonicated and filtered through the Whatman filter paper. Finally, the obtained I-Fe_3O_4-NBC were characterized by various analytical techniques and employed to remove heavy metals from the aqueous solution.

2.5 Characterization of I-Fe_3O_4-NPs, and I-Fe_3O_4-NBC

The synthesized I-Fe_3O_4-NPs and I-Fe_3O_4-NBC were characterized using advanced analytical techniques, i.e., UV–visible, FT-IR, SEM, and XRD. Morphological characters of I-Fe_3O_4-NPs and I-Fe_3O_4-NBC were analyzed by scanning electron microscope (SEM) model JSM-6380 (JEOL Electronics Company, Japan). Similarly, the crystal structure was

studied by X-ray diffraction (D-8 of Bruker). The spectrophotometric study for the confirmation of I-Fe_3O_4-NPs was conducted by a double-beam UV–visible spectrophotometer (UV-2600, Shimadzu, Japan). FT-IR spectra of I-Fe_3O_4-NPs nanoparticles and their composites in the range of 400–4000 cm^{-1} were obtained by FT-IR spectrophotometer Thermo Electron Scientific (Madison, WI, USA) with a KBr pellet. The size and shape of I-Fe_3O_4-NPs and I-Fe_3O_4-NBC was confirmed by atomic force microscope (Agilent, Santa Clara, CA, USA). AFM imaging was performed on the NanoScope V system (Bruker Ltd, Germany). Dynamic light scattering (DLS) and zeta potential measurements were taken for particle size and adsorption activity of adsorbent using the laser scattering particle size distribution analyzer (Horiba Scientific, Kyoto, Japan) and the zeta potential analyzer (ELSZ-2000), respectively. Furthermore, a salt addition method was used to determine the point of zero charges (isoelectric point) of the adsorbent, as reported elsewhere [53].

2.6 Procedures for Batch Adsorption Studies

The batch adsorption experiments were performed by varying the operation parameters, i.e., pH (2.0–12.0), I-Fe_3O_4-NBC dose (0.10–0.50 g), temperature (20–90 °C), initial concentration of Cd, Ni, and Pb (2.0–30.0 mg L^{-1}), and contact time (10–60 min). The resulting samples were centrifuged at 800 rpm for about 10 min to separate the adsorbent (I-Fe_3O_4-NBC) from the experimental solution. The samples were filtered by Whatman filter paper No. 42. Finally, Cd, Ni, and Pb residual concentrations were measured by flame atomic absorption spectrometry (AAS; Hitachi, Tokyo, Japan) [5, 8].

The adsorption capacity (q_e) is the amount (mg) of the adsorbates (Cd, Ni, and Pb) adsorbed per unit mass (g) of adsorbent (I-Fe_3O_4-NBC) and was calculated as given in Eq. 1.

$$q_e = \frac{(C_i - C_f) \times V}{m} \quad (1)$$

Here 'q_e' is the experimental adsorption capacity, whereas 'C_i' and 'C_e' are the initial and final/equilibrium concentrations. Moreover, 'm' is the dried mass of adsorbent (I-Fe_3O_4-NBC), and 'V' stands for the solution volume (L).

2.7 Sampling of water samples

Drinking water (surface and groundwater) samples were randomly collected using the cluster sampling method from Manchar lake (26.428° N:67.673° E), Khairpur district (26.0°–27.75° N:68.0°–68.25° E), district Umarkot (25.370° N:69.730° E), and Dadu city (26.732° N:67.779°) during May and June followed the SOPs of COVID-19 conditions with the assistance of local NGOs. Surface water samples (n = 10) of Manchar Lake were sampled from the core stream of three to four different sampling stations at an approximate depth of 20–25 cm. The groundwater samples (n = 50) of the hand pump (about 15–20 m of depth) of selected study areas have been sampled. The surface water sampling was carried out in 1.5 L capacity Van Dorn plastic bottles, stored in well-stoppered polyethylene synthetic bottles formerly soaking in 10% HNO_3 overnight, and then washed with deionized water. Collected water samples were kept under cool conditions in an ice cooler and transported to the laboratory on the same sampling day, as reported elsewhere [54]

3 Results and Discussion

3.1 Characterization of Biosynthesized I-Fe_3O_4-NPs and I-Fe_3O_4-NBC

The UV–visible analysis is an important and quite sensitive characterization approach for the evaluation of nanoparticles [31, 55]. UV–visible spectral scanning method was used to confirm the synthesis of biosynthesized I-Fe_3O_4-NPs. The intense peak observed at 274 nm confirmed the presence of Fe_3O_4-NPs. The broadening of the peak may refer to the various particle size distribution (Fig. 1a).

FT-IR spectroscopy was also carried out for the confirmation of I-Fe_3O_4-NPs and I-Fe_3O_4-NBC in the range 400–4000 cm^{-1} (Fig. 1b). The peaks around ~ 3371, ~ 1643 cm^{-1} are due to stretching and bending vibrations of O–H group, respectively [31, 56]. Moreover, the peak at 577 cm^{-1} is due to Fe–O stretching, which confirms the presence of I-Fe_3O_4-NPs. In the FT-IR spectrum, I-Fe_3O_4-NBC showed broadband at ~ 3421 cm^{-1}, which might be due to the stretching vibration of O–H and N–H functionalities present in chitosan (natural polymer). Moreover, the peaks at ~ 1643 and ~ 1560 cm^{-1} are attributed to O–H and N–H bending vibrations, respectively [31, 56], which confirmed the chitosan coating over the I-Fe_3O_4-NPs. The strong peak appeared at 1088 cm^{-1}, possibly due to stretching vibrations of the C–O–C bond of chitosan (polysaccharide) [57]. The peak at 577 cm^{-1} is due to the Fe–O bond [58], which may be associated with the –NH_2 group of chitosan functionality. The FT-IR characterization showed an excellent adsorption behavior of I-Fe_3O_4-NBC for the removal of TMs based on its high hydrophilicity associated with –OH groups of glucose and –NH_2 (acetamido, primary amino) of chitosan (Fig. 2). Thus, the proposed I-Fe_3O_4-NBC adsorbent can adsorb TMs from the contaminated water due to high chemical reactivity of these groups and the flexible structure of associated the polymer chain of chitosan [21]. Similar behavior of chitosan nanocomposites was also reported for removing Cu(II) and Zn(II) from contaminated water [59, 60].

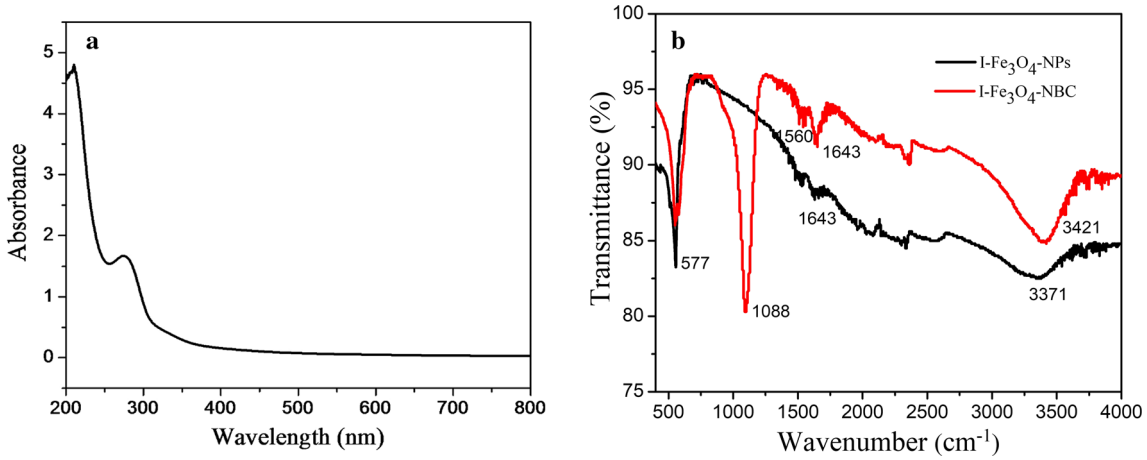

Fig. 1 **a** UV–visible and **b** FT-IR spectroscopic response of I-Fe_3O_4-NPs and I-Fe_3O_4-NBC

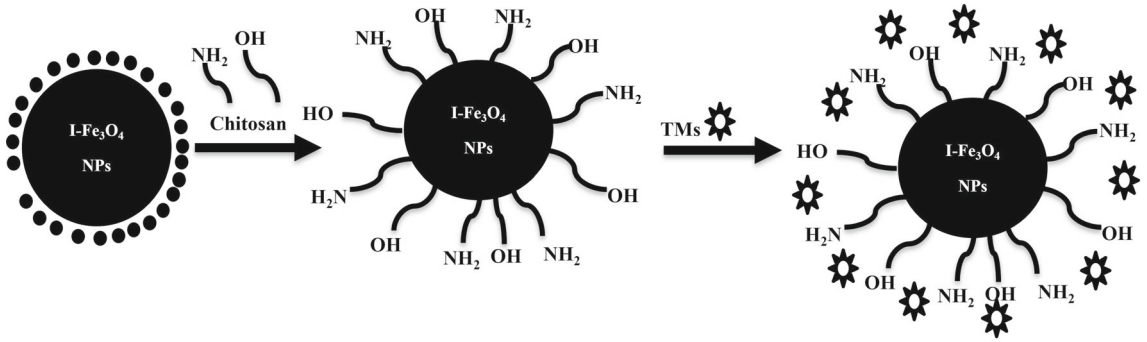

Fig. 2 Possible mechanism for the removal of TMs by I-Fe_3O_4-NBC

Scanning electron microscopic (SEM) analysis was carried out to study the structural morphology of the synthesized I-Fe_3O_4-NPs and I-Fe_3O_4-NBC. Figure 3a shows an SEM topographic image of I-Fe_3O_4-NPs synthesized by $FeCl_3.6H_2O$ and $Fe_2SO_4.7H_2O$ using *Ixora coccinea* plant leaf extract. The SEM images of I-Fe_3O_4-NPs showed a quasi-spherical shape and appeared in the form of clusters (Fig. 3a). The particles are agglomerated with each other and have a rough and porous surface. The SEM topographic images of the I-Fe_3O_4-NBC are given in Fig. 3b. The structural morphology of I-Fe_3O_4-NPs has changed with the addition of chitosan. The accumulation of chitosan over the I-Fe_2O_3-NPs with a uniform granular, porous surface is shown in Fig. 3b. It may be due to the chitosan polymer chains which can enclose the I-Fe_3O_4-NPs, and the I-Fe_3O_4-NBC may grow as multiparticle. Moreover, the sizes of particles have also increased. It confirmed the successful fabrication of I-Fe_3O_4-NBC.

The X-ray diffraction (XRD) was carried out to study the structural characteristics of biosynthesized I-Fe_3O_4-NPs and I-Fe_3O_4-NBC. XRD spectrum I-Fe_3O_4-NPs showed six different diffraction peaks at the diffraction angle (2θ): 30.22, 35.60, 45.06, 54.10,57.68, and 63.10, corresponding to the reflection planes (220), (311), (222), (400), (422) and (511), respectively (Fig. 3c). The array of lattice planes indexed to the magnetite's pure cubic phase and well matched with Joint Committee on Powder Diffraction Standards (JCPDS) card No. 19-0629 [61]. These diffraction peaks illustrated the crystalline nature of the particles. However, there was no XRD peak detected for the impurities. However, the same peaks were observed in the XRD spectrum of I-Fe_3O_4-NBC. The intensity of the peaks had decreased, indicating the chitosan coating did not destroy the crystalline behavior of nanoparticles. Moreover, the Debye–Scherrer equation (Eq. 2) was used to calculate the average crystallite sizes [62] of I-Fe_3O_4-NPs and I-Fe_3O_4-NBC, which were obtained 1.32 and 6.80 nm for I-Fe_3O_4-NPs and I-Fe_3O_4-NBC, respectively. In this equation (given below), D shows the average crystallite size, k is the shape constant of the crystal, λ is the wavelength X-ray source, β shows the peak width at half of the maximum intensity, and θ shows the Bragg diffraction angle.

$$D = \frac{k\lambda}{\beta \cdot \cos\theta} \tag{2}$$

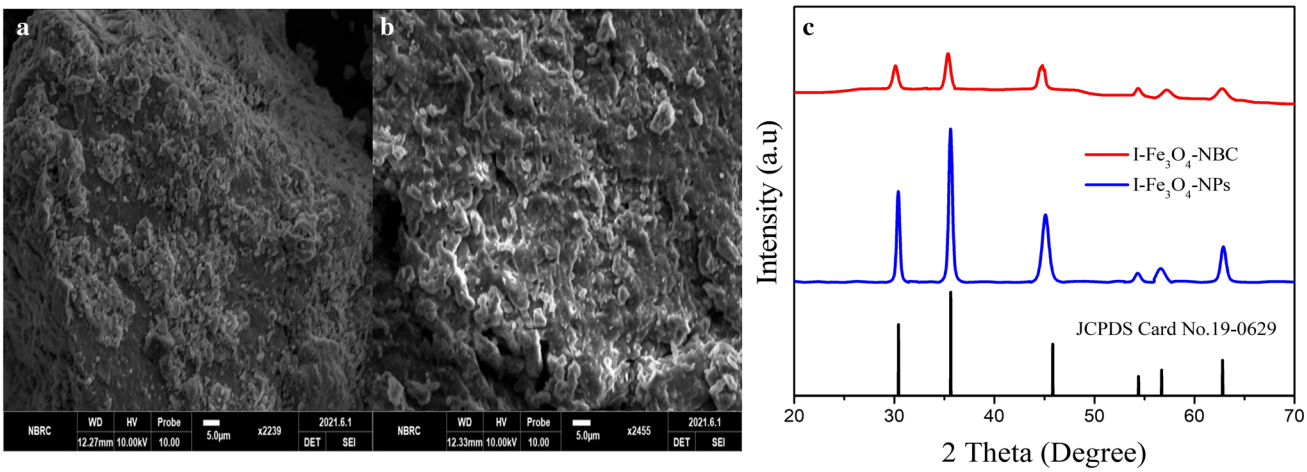

Fig. 3 SEM image of **a** I-Fe_3O_4-NPs, **b** I-Fe_3O_4-NBC and XRD responses

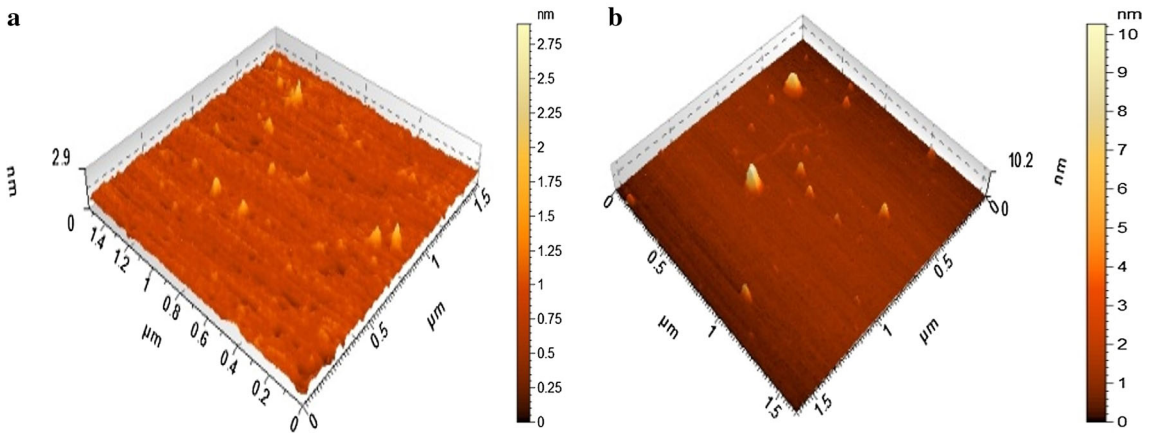

Fig. 4 AFM images of **a** I-Fe_3O_4-NPs, **b** I-Fe_3O_4-NBC

3.1.1 Atomic Force Microscopy (AFM) Study

The technology of atomic force microscopy (AFM) is an essential biophysical tool for analyzing the morphology and size of nanoparticles and biomolecules [63]. The height and the structure of the I-Fe_3O_4-NPs were investigated with AFM (Fig. 4a). The AFM images show the aggregation of I-Fe_3O_4-NPs with a rough surface. The particles are non-spherical, with particle sizes of 1.45–2.61 nm. Moreover, the AFM images of I-Fe_3O_4-NBC showed the successful covering of chitosan over the I-Fe_3O_4-NPs with an oval shape and particle size of 4.6–10.3 nm (Fig. 4b). This may indicate the enhancement in the shape and particle size of I-Fe_3O_4-NBC as compared to I-Fe_3O_4-NPs for its successful synthesis.

3.1.2 Size and Zeta Potential Distribution of Biosynthesized Fe_3O_4 NPs

The 55.0 mg of synthesized nanoparticle suspensions in 6.0 mL of deionized water (pH 7) was treated with a 10-min ultrasonic treatment for DLS and zeta potential experiments. The zeta potential and zeta size of I-Fe_3O_4-NBC dispersion in water are shown in Fig. 5a. The zeta size of I-Fe_3O_4-NBC was found from 9 to 14 nm with an average particle size of 11.3 nm. Zeta potential distribution is used to measure the stability of particles of an adsorbent material [1]. In addition, the size distribution values of I-Fe_3O_4-NBC by DLS are comparable, with slight variation from those observed by the AFM and estimated by the XRD study ($p > 0.05$). The slightly large particle size might be followed by DLS, which showed the hydrodynamic size of particles and their surrounding diffuse layer [64]. The zeta potential of biosynthesized I-Fe_3O_4-NBC was found to be − 40.7 mV (Fig. 5b). The substance with zeta potential values of less than − 30 mV and greater than + 30 mV is considered strongly anionic and strongly cationic, respectively [65]. The negatively charged zeta potential values (− 40.7 mV) of I-Fe_3O_4-NBC participated in the electrostatic stability of the biosynthesized I-Fe_3O_4-NBC. The intensive signal at − 40.69 mV revealed that the biosynthesized nanoparticles have negative surface

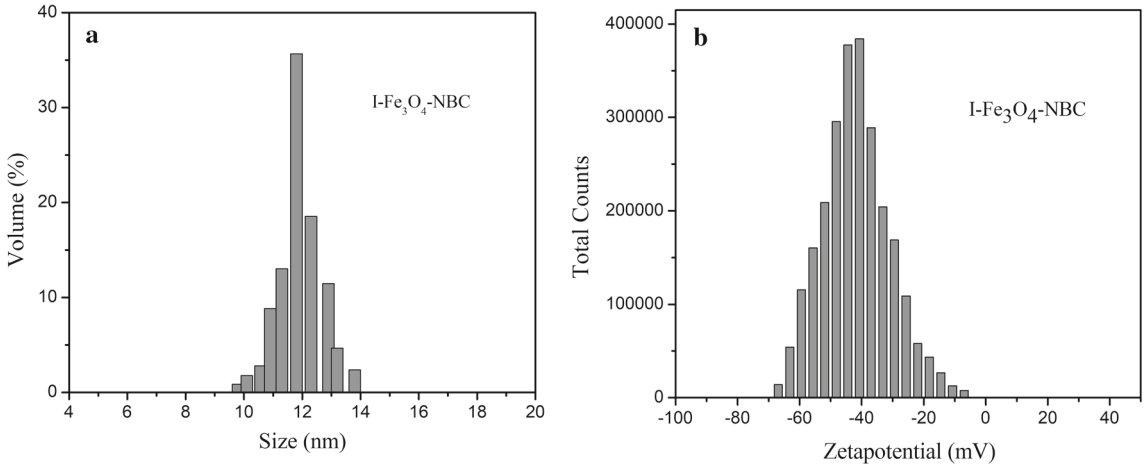

Fig. 5 **a** Size distribution, **b** zeta potential of I-Fe_3O_4-NBC

charges. A zeta potential value of − 40.69 mV indicates that the dispersed I-Fe_3O_4-NBC was capped by negatively charged groups proving that they are stable.

3.2 Optimization of Affecting Parameters on the Adsorption Behavior for Cd, Ni, and Pb by I-Fe_3O_4-NBC

The different parameters of the batch (adsorption) experiment, i.e., pH of the solution, adsorbent dosage, analyte concentration, contact time, and temperature, were optimized to get maximum adsorption capacity of biosynthesized I-Fe_3O_4-NBC for removal of Cd, Ni, and Pb from the aqueous solution.

3.2.1 Effect of pH

The adsorption of TMs may depend on the pH and could be justified by the perception of surface chemistry in an aqueous phase. The effect of solution pH in the range of 2.0–12.0 for the removal of Cd, Ni, and Pb by I-Fe_3O_4-NBC at a constant sorbent dosage of 0.3 mg, shaking time 20 min and 303 K is listed in Fig. 6a. The surfaces of I-Fe_3O_4-NBC may be enclosed with polar functionality of chitosan as found in FT-IR study (Fig. 1b) which may lead to change the adsorption of Cd, Ni, and Pb with change in pH of the solution. Meanwhile, the point of zero-charge (pH_{pzc}) study showed that the surface charge on I-Fe_3O_4-NBC is neutral at pH_{pzc} (pH 5.80) as described in the literature [66]. Based on the findings below this point (pH < 6.0), the I-Fe_3O_4-NBC surface is positively charged and repealed Cd, Ni, and Pb (cations). However, at pH > pH_{pzc} value, the I-Fe_3O_4-NBC surface is negatively charged, so the Cd, Ni, and Pb adsorption could occur by simple electrostatic attraction. Thus, the adsorption of Cd, Ni, and Pb from the aqueous solution by I-Fe_3O_4-NBC with increased pH. Cd, Ni, and Pb adsorption reached the maximum between pH 7.0 and 10, but the difference is very small. Therefore, pH 7.0 was selected for further study.

3.2.2 Effects of Analyte Concentration

The efficiency of adsorption was affected by initial analyte concentration [67]. Therefore, the effect of Cd, Ni, and Pb concentration on their adsorption by I-Fe_3O_4-NBC in the aqueous solution was studied. The adsorption behavior of 0.3 g in 100 mL of deionized water of I-Fe_3O_4-NBC for different concentrations of Cd, Ni, and Pb ranged from 2 to 40 mg L^{-1} at pH 7.0 (Fig. 1b). The adsorption of Cd, Ni, and Pb at low concentration (2.0 to 8) was found in the range of 95 to 97%. However, the maximum adsorption (up to 97%) of Cd, Ni, and Pb was obtained at 10 mg L^{-1} (Fig. 6b). The removal of Cd, Ni, and Pb was decreased by a further increase in their concentration (> 10 mg L^{-1}). It may be due to the saturation of Cd, Ni, and Pb at higher concentrations and the unavailability of an active adsorbent site on the surface of the adsorbent (I-Fe_3O_4-NBC) [68, 69]. Thus, an initial concentration of 10 mg L^{-1} was selected as the optimum concentration for the maximum adsorption of Cd, Ni, and Pb.

3.2.3 Effect of Adsorbent Dosage

The effect of I-Fe_3O_4-NBC dose in the range of 0.1–0.5 g was also studied for the adsorption of Cd, Ni, and Pb ions. It was observed that the adsorption of Cd, Ni, and Pb from an aqueous solution was increased with an increase in the dose of I-Fe_3O_4-NBC at pH 7.0. After 0.3 g, further increase in adsorbent dose has not affected the adsorption of Cd, Ni, and Pb, and % adsorption remained constant (Fig. 6c). This is possible because the presence of chitosan in I-Fe_3O_4-NBC reduces the particle aggregation of I-Fe_3O_4-NPs and leads to an increase in the adsorption surface. Moreover, the presence

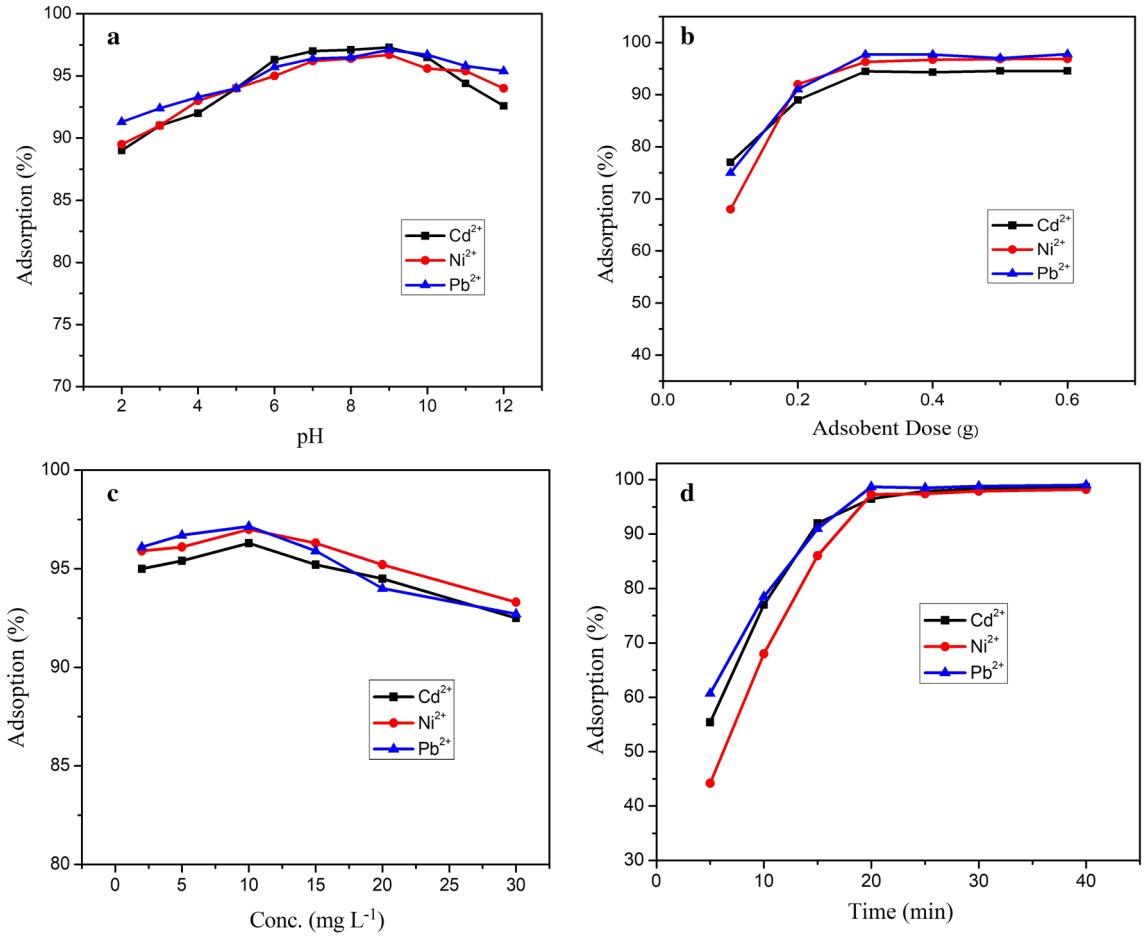

Fig. 6 Effect of **a** pH, **b** dosage of I-Fe_3O_4-NBC, **c** concentration of Cd^{2+}, Ni^{2+}, and Pb^{2+}, and **d** contact time on the adsorption of Cd^{2+}, Ni^{2+}, and Pb^{2+} from the aqueous solution

of NH_2 functional groups of chitosan on the surface of I-Fe_3O_4-NBC which are responsible for the adsorption of Cd, Ni, and Pb [66]. When the adsorbent dosage was below the optimum value (0.3 g), the removals of target metal ions were low due to the availability of fewer binding sites. As the maximum adsorption was observed at 0.3 g, it was chosen as the optimal adsorbent dose for removing target metals [70].

3.2.4 Effect of Contact Time

The contact time is one of the most effective factors in the batch adsorption process [71, 72]. Therefore, the effect of contact time was investigated on the adsorption of Cd, Ni, and Pb (10 mg L^{-1}) by I-Fe_3O_4-NBC in the range of 5–40 min at 303 K (Fig. 6d). The adsorption of Cd, Ni, and Pb by I-Fe_3O_4-NBC from the aqueous solution was increased from 5 to 20 min (up to 98%). Thus, the proposed adsorbent (I-Fe_3O_4-NBC) has many vacant active sites (–NH_2/–OH), which are confirmed the adsorption of TMs. Cd, Ni, and Pb adsorption almost remained constant, and the percentage adsorption difference between 20 and 60 min was less than 1% [73]. Therefore, a steady-state approximation was assumed to save time, and a quasi-equilibrium situation was considered at 20 min of contact time.

3.2.5 Effect of Temperature

The effect of temperature on the adsorption of Cd, Ni, and Pb by I-Fe_3O_4-NBC was studied by conducting a set of different experiments at an initial concentration (10 mg L^{-1}), and 0.3 g of I-Fe_3O_4-NBC at different temperatures, i.e., 298, 303, 313, 323, 333, and 343 K. The adsorption of Cd, Ni, and Pb on I-Fe_3O_4-NBC was from 298 to 303 K, revealing that the adsorption process was exothermic. But there is a decrease in the efficiency of adsorption above 313 K. The temperature study showed that 303 K temperature showed high adsorption of TMs, which may have great feasibility to remove the TMs contamination at normal ambient temperature even in our laboratories or large-scale without the need for energy/fuel consumption for heating.

Table 1 Analytical results of isotherm, kinetics, and thermodynamic parameters of Cd, Ni, and Pb on I-Fe_3O_4-NBC

Isotherm study									
Langmuir model				Freundlich model			D–R model		
Metal	Q (mM g^{-1})	B (L mM^{-1})	R^2	Cm (mM g^{-1})	n	R^2	X_m (M g^{-1})	E (kJ M^{-1})	R^2
Cd	0.072	2.03	0.8501	0.0072	0.631	0.9793	13.11	41.7	0.9556
Pb	0.702	0.171	0.9281	0.0089	0.756	0.8606	9.020	17.4	0.9325
Ni	0.096	7.95	0.9128	0.9128	0.789	0.9793	8.47	17.9	0.9303

Kinetics study						
	Pseudo-first order			Pseudo-second order		
	k_1 (min^{-1})	Q_e (mM g^{-1})	R^2	k_2 (g mM^{-1} min^{-1})	q_e (mM g^{-1})	R^2
Cd	4.610	1.070	0.9734	0.0625	4.00	0.993
Pb	1.403	1.026	0.8718	0.0252	3.972	0.9292
Ni	0.439	1.154	0.9818	0.0415	2.409	0.9999

Thermodynamic study									
	Cd			Pb			Ni		
T K	$\Delta G°$ kJ M^{-1}	$\Delta H°$	$\Delta S°$ kJ M^{-1} K^{-1}	$\Delta G°$ kJ M^{-1}	$\Delta H°$	$\Delta S°$ kJ M^{-1} K^{-1}	$\Delta G°$	$\Delta H°$	$\Delta S°$ kJ M^{-1} K^{-1}
303	− 8.4	− 48.13	0.1862	− 8.6	− 48.20	0.186	− 8.8	− 48.21	0.0125
313	− 9.7			− 9.0			− 8.6		
323	− 12.2			− 12.2			− 8.0		
333	− 12.4			− 8.8			− 4.1		
343	− 10.8			− 9.1			− 0.3		
353	− 11.5			− 9.7			2.2		

3.3 Isotherm Studies of I-Fe_3O_4-NBC

The linear form adsorption isotherm was applied to examine the adsorption of TMs on the synthesized adsorbent (I-Fe_3O_4-NBC) to understand the adsorption process. The linear equations for the Langmuir, Freundlich and Dubinin–Radushkevich (D–R) isotherm are given in Eqs. 3, 4, and 5, respectively. Moreover, the summary of the adsorption parameters of studied isotherm models (Langmuir, Freundlich, and D–R isotherm) is given in Table 1. According to the Langmuir isotherm, adsorbate forms a uniform monolayer on the surface of the adsorbent, and no more adsorption takes place due to a limited number of identical sites [74]. Freundlich model suggests that multilayer of TMs adsorption takes place on the heterogeneous the surface of Fe_3O_4-NBC and does not restrict to monolayer as the Langmuir model. Compared to the Langmuir isotherm model, the Freundlich isotherm model better fit the TMs adsorption on I-Fe_3O_4-NBC with R^2 values of 0.9793, 0.9753, and 0.8606 for Cd, Ni, and Pb, respectively. The D–R isotherms provide important information regarding the energy parameters, which have R^2 values of 0.9556, 0.9303, and 0.9325 for Cd, Ni, and Pb, respectively. The heats of adsorption were obtained as 41.66, 17.85, and 17.36 kJ mol^{-1} for Cd, Ni, and Pb by I-Fe_3O_4-NBC, respectively. The heat of adsorption was found to be > 8.0 kJ mol^{-1}, suggesting that the adsorption of TMs is a chemical phenomenon [75]. The Freundlich isotherm is best fitted with TMs adsorption data among all the adsorption isotherms. It showed that multilayer adsorption on the I-Fe_3O_4-NBC surface was responsible for the adsorption process. The process of TMs adsorption is chemical.

$$\frac{C_e}{q_e} = \frac{1}{Q^0 b} + \frac{C_e}{Q^0} \tag{3}$$

$$\ln q_e = \ln C_m + \frac{1}{n} \ln C_e \tag{4}$$

$$\ln q_e = \ln X_m - \beta F^2 \tag{5}$$

3.4 Adsorption Kinetic Models

The adsorption rate of TMs on I-Fe_3O_4-NBC has been investigated using pseudo-first- and pseudo-second-order kinetic models to determine the adsorption behavior. The rate equations for pseudo-first and pseudo-second order are given in Eqs. 6 and 7, respectively. The experimental parameters for pseudo-first- and pseudo-second-order reactions are listed in Table 1. In the case of pseudo-first-order kinetics, R^2 was found at 0.9734, 0.9818, and 0.8718 for Cd, Ni, and Pb, respectively. Moreover, R^2 values of pseudo-second-order kinetics for Cd, Ni, and Pb were found to be 0.9922, 0.9978, and 0.9292, respectively. Thus, it is suggested that the pseudo-second-order model is best fitted to explain the adsorption kinetics of TMs on the I-Fe_3O_4-NBC.

$$\log(q_e - q_t) = \log(q_e) - \frac{k1t}{2.303} \tag{6}$$

$$\frac{t}{q_t} = \frac{1}{k2q_e^2} + \frac{1}{q_e}t \tag{7}$$

3.4.1 Thermodynamic Study

The influence of temperature ranging from 303 to 323 K was observed to assess the adsorption in the optimum conditions. The changes in the thermodynamic parameters, i.e., Gibb's free energy ($G°$), enthalpy ($H°$), and entropy ($S°$), during the adsorption process of TMs on I-Fe_3O_4-NBC are given in Table 1, and these parameters were calculated using Eqs. 8 and 9.

$$\Delta G^{\circ} = -RT \ln K_o \tag{8}$$

$$\ln K_0 = -\left(\frac{\Delta H^{\circ}}{R}\frac{1}{T} + \frac{\Delta S^{\circ}}{R}\right) \tag{9}$$

As $\Delta H°$ and $\Delta G°$ have negative values, it demonstrates that the adsorption of TMs is exothermic and spontaneous (Table 1). Entropy change is also negative, which suggests that little change in the basic structure of I-Fe_3O_4-NBC happened throughout the biosorption processes [75]. Therefore, the adsorbed ions are relatively stable on the solid surface and cause a loss of degrees of freedom at the solid/liquid contact. Moreover, it has been demonstrated that TMs absorption decreased as the temperature rose, indicating the spontaneous nature of adsorption.

A comparative assessment of adsorption characteristics of understudied nanoadsorbent (I-Fe_3O_4-NBC) with those research studies reported in the literature for the removal of TMs is listed in Table 2. This assessment comparison indicated that the fabricated I-Fe_3O_4-NBC might have comparable adsorption capacity for simultaneous removal of TMs under a wide range of pH from the surface and groundwater samples [76–81]. Thus, the proposed nanomaterial can be utilized under optimum conditions for the simultaneous removal of TMs in large-scale applications to purify surface and groundwater.

3.4.2 Application of Proposed I-Fe_3O_4-NBC

The proposed I-Fe_3O_4-NBC was satisfactorily used for the simultaneous removal of Cd, Ni, and Pb from contaminated Manchar Lake water and groundwater in three different areas (Khairpur, Umarkot, and Dadu districts). The mean results of TMs removal before and after adsorption by I-Fe_3O_4-NBC from the studied surface and groundwater samples are listed in Table 3. The studied surface and groundwater samples were highly contaminated with TMs and excessed the WHO permissible limit for drinking water (3.0 (Cd), 20 (Ni), and 10 (Pb) $\mu g\ L^{-1}$) due to anthropogenic and geological sources. After adsorption by I-Fe_3O_4-NBC, the %removal of TMs was to be greater than 94.0% in both surface and groundwater samples. The difference in the adsorption behavior of TMs might be due to the presence of multicomponent impurities along with TMs.

Biosynthesis of the iron oxide nanoparticles (I-Fe_3O_4-NP) using *Ixoro coccinea* leaf extract proved that the adsorption capacity of TMs was more significant when compared to previously reported work [77–81]. The current study shows that the adsorption process by I- Fe_3O_4-NC follows the Freundlich isotherm model to remove Cd, which was different from previously reported findings [79, 80]. In contrast, proposed adsorption may follow the Langmuir isotherm similar like previous studies [79, 80]. The maximum adsorption capacity using proposed nanobiocomposites for Pb was 66.4 mg g^{-1}, which was found to be greater than reported in the literature [76]. The proposed adsorption process was best fitted to follow pseudo-second-order kinetics and showed an exothermic, favorable, and spontaneous nature than the reported work [76]. In addition, I-Fe_3O_4-NBC is novel based on its application for simultaneous adsorption of Cd, Ni, and Pb from surface and groundwater as compared to the reported materials [77–81]. It was observed that the proposed nanobiocomposite is most efficient in removing TMs from drinking water up to its recommended permissible limit (Table 2).

4 Conclusions

The proposed I-Fe_3O_4-NPs were successfully synthesized from the leaf extract of *Ixora coccinea* and confirmed by different analytical techniques. The fabrication of I-Fe_3O_4-NBC was proved by the FT-IR study, which indicates that the amine and hydroxyl groups of chitosan formed the stable composite with I-Fe_3O_4-NPs. The proposed adsorbent

Table 2 Comparison of adsorption efficiency of the proposed I-Fe_3O_4-NBC with the literature

Composite material	Isotherms model	Adsorption capacity (mg g^{-1})	Thermodynamics	Reaction kinetics	pH	Metal	Time (min)	References
Magnetic NiO/Biochar	Freundlich isotherm	28.0	Exothermic		6.4	Pb	240	[76]
Chitosan–iron (III) composite	Langmuir isotherm	373	–	Pseudo-second	4.8	Pb	2880	[77]
		112				Hg (II)		
Magnetite nanobiocomposite/chitosan	Langmuir isotherm	192	–	Pseudo-second	8.2	Pb	90	[78]
Iron dust–zeolite/chitosan	Langmuir isotherm	78.1	Endothermic	–	6.9	Cd	60	[79]
	Freundlich isotherm	76.3				Ni		
Chitosan-coated zero-valent iron	Langmuir isotherm	667	Endothermic	Pseudo-second	5.0	Pb	150	[80]
Zero-valent iron/chitosan	Langmuir isotherm	143	–	Pseudo-second	7.0	Cd	90	[81]
I-Fe_3O_4-NBC	Freundlich isotherm for Cd and Ni while Langmuir isotherm for Pb	66.0 (Cd), 60 (Ni), and 66.4 (Pb)	Exothermic	Pseudo-second	(7.0–10)	Cd/Ni/Pb	20	This study

Table 3 Results of Cd, Pb, Ni concentration before and after adsorption by I-Fe_3O_4-NBC

Metals	Surface water ($n = 10$)	Ground water ($n = 50$)		
	Manchar Lake	Khairpur Mir's ($n = 25$)	Umar Kot ($n = 15$)	Dadu ($n = 10$)
Cd ($\mu g\ L^{-1}$) *3 $\mu g\ L^{-1}$				
Before adsorption	6.80 ± 1.75	2.40 ± 0.300	4.40 ± 0.32	2.80 ± 0.260
After adsorption	0.30 ± 0.03	0.11 ± 0.02	0.19 ± 0.03	0.12 ± 0.02
% removal	94.0–96.1	95.1–96.0	95.3–95.2	95.4–96.1
Pb ($\mu g\ L^{-1}$) *10 $\mu g\ L^{-1}$				
Before adsorption	82.2 ± 6.70	14.8 ± 4.03	18.2 ± 3.55	15.5 ± 4.44
After adsorption	2.40 ± 0.33	0.52 ± 0.23	0.81 ± 0.32	0.45 ± 0.23
% removal	96.9–97.2	96.1–97.3	94.8–96.7	96.6–98.1
Ni ($\mu g\ L^{-1}$) *20 $\mu g\ L^{-1}$				
Before adsorption	28.6 ± 7.50	25.6 ± 5.8	30.8 ± 3.55	22.8 ± 4.12
After adsorption	1.10 ± 0.25	1.02 ± 0.13	0.82 ± 0.22	1.02 ± 0.34
% removal	95.0–96.2	95.5–96.3	96.9–97.8	94.9–96.3

*WHO permissible limit

I-Fe_3O_4-NBC showed good removal of TMs in pH between 7 and 10, with the maximum at pH 7 ($p > 0.05$). Thus, I-Fe_3O_4-NBC was applied at neutral pH and temperature (30 °C) for the excellent removal of TMs (> 95%) with adsorption capacities 66.0, 60.0, and 66.4 mg g^{-1} for Cd, Ni, and Pb, respectively. The adsorption process follows the Freundlich isotherm model by I-Fe_3O_4 NBC for removal of Cd, and Ni, while the Pb may be adsorption followed by monolayer surface coverage. The adsorption of TMs on I-Fe_3O_4-NBC followed the pseudo-second-order kinetics. The thermodynamic studies showed the feasibility, spontaneity, and exothermic nature of the adsorption process of TMs removal by I-Fe_3O_4-NBC. According to the mean free energy values obtained from the D–R isotherm model, chemisorptions primarily caused the adsorption. It is concluded that the metal ion adsorption on the surface of I-Fe_3O_4-NBC was significant (> 95%) because of $–NH_2$ and –OH active adsorptive sites of chitosan interacting with metal ions.

Acknowledgements All authors appreciatively acknowledge the Higher Education Commission (HEC.) Islamabad, Pakistan, for project grants as project No. 8147/Sindh/NRPU/R&D/HEC/2017 and the National Centre of Excellence in Analytical Chemistry, University of Sindh, Jamshoro, for the partial financial assistance of the current study. The authors also acknowledge the Young Welfare Society Sindh for their help for collecting the drinking water samples from different districts of districts Jamshoro and Hyderabad.

Declarations

Conflict of interest It has been declared that the proposed research study was done for non-commercial and educational purposes and could not be interpreted as any possible conflict of interest.

References

1. Ali, I., et al.: Chiral analysis of ibuprofen residues in water and sediment. Anal. Lett. **42**(12), 1747–1760 (2009)
2. Ali, I.; Jain, C.: Groundwater contamination and health hazards by some of the most commonly used pesticides. Curr. Sci. **75**(10), 1011–1014 (1998)
3. Tanzifi, M., et al.: Artificial neural network optimization for methyl orange adsorption onto polyaniline nano-adsorbent: kinetic, isotherm and thermodynamic studies. J. Mol. Liq. **244**, 189–200 (2017)
4. Ayangbenro, A.S.; Babalola, O.O.: A new strategy for heavy metal polluted environments: a review of microbial biosorbents. Int. J. Environ. Res. Public Health **14**(1), 94 (2017)
5. Junejo, S.H., et al.: Cadmium and lead hazardous impact assessment of pond fish species. Biol. Trace Elem. Res. **191**(2), 502–511 (2019)
6. Rahmat, M., et al.: Highly efficient removal of crystal violet dye from water by MnO2 based nanofibrous mesh/photocatalytic process. J. Mark. Res. **8**(6), 5149–5159 (2019)
7. Ferronato, N.; Torretta, V.: Waste mismanagement in developing countries: a review of global issues. Int. J. Environ. Res. Public Health **16**(6), 1060 (2019)

8. Baig, J.A., et al.: Evaluation of arsenic, cadmium, nickel and lead in common spices in Pakistan. Biol. Trace Elem. Res. **187**(2), 586–595 (2019)
9. Fang, X., et al.: Internal pore decoration with polydopamine nanoparticle on polymeric ultrafiltration membrane for enhanced heavy metal removal. Chem. Eng. J. **314**, 38–49 (2017)
10. Ricci, B.C., et al.: Integration of nanofiltration and reverse osmosis for metal separation and sulfuric acid recovery from gold mining effluent. Sep. Purif. Technol. **154**, 11–21 (2015)
11. Fu, F., et al.: Application of a novel strategy—advanced Fenton-chemical precipitation to the treatment of strong stability chelated heavy metal containing wastewater. Chem. Eng. J. **189**, 283–287 (2012)
12. Sharma, G., et al.: Fabrication and characterization of sodium dodecyl sulphate@ ironsilicophosphate nanocomposite: Ion exchange properties and selectivity for binary metal ions. Mater. Chem. Phys. **193**, 129–139 (2017)
13. Awual, M.R., et al.: Facile mercury detection and removal from aqueous media involving ligand impregnated conjugate nanomaterials. Chem. Eng. J. **290**, 243–251 (2016)
14. Naushad, M., et al.: Nickel ferrite bearing nitrogen-doped mesoporous carbon as efficient adsorbent for the removal of highly toxic metal ion from aqueous medium. Chem. Eng. J. **330**, 1351–1360 (2017)
15. Rimu, S.H.; Rahman, M.M.: Insight of chitosan-based nanocomposite for removal of hexavalent chromium from wastewater—a review. Int. J. Environ. Anal. Chem. (2020). https://doi.org/10.1080/03067319.2020.1817426
16. Al-Shaalan, N.H., et al.: High performance removal and simulation studies of diuron pesticide in water on MWCNTs. J. Mol. Liq. **289**, 111039 (2019)
17. Amer, M.W.; Awwad, A.M.: Green synthesis of copper nanoparticles by *Citrus limon* fruits extract, characterization and antibacterial activity. Chem. Int. **7**(1), 1–8 (2021)
18. Yadav, V.K., et al.: Microbial synthesis of nanoparticles and their applications for wastewater treatment. In: Singh, J.; Vyas, A.; Wang, S.; Prasad, R. (Eds.) Microbial Biotechnology: Basic Research and Applications, pp. 147–187. Springer, Berlin (2020)
19. Ali, I., et al.: Advances in carbon nanomaterials as lubricants modifiers. J. Mol. Liq. **279**, 251–266 (2019)
20. Rai, P.K., et al.: A critical review of ferrate (VI)-based remediation of soil and groundwater. Environ. Res. **160**, 420–448 (2018)
21. Dave, P.N.; Chopda, L.V.: Application of iron oxide nanomaterials for the removal of heavy metals. J. Nanotechnol. **2014**, 1–14 (2014)
22. Cai, J., et al.: Organic additive-free synthesis of mesocrystalline hematite nanoplates via two-dimensional oriented attachment. CrystEngComm **16**(8), 1553–1559 (2014)
23. Pulit-Prociak, J.; Stokłosa, K.; Banach, M.: Nanosilver products and toxicity. Environ. Chem. Lett. **13**(1), 59–68 (2015)
24. Mondal, P.; Anweshan, A.; Purkait, M.K.: Green synthesis and environmental application of iron-based nanomaterials and nanocomposite: a review. Chemosphere **259**, 127509 (2020)
25. Leonard, K., et al.: In situ green synthesis of biocompatible ginseng capped gold nanoparticles with remarkable stability. Colloids Surf B Biointerfaces **82**(2), 391–396 (2011)
26. Santhoshkumar, T., et al.: Green synthesis of titanium dioxide nanoparticles using *Psidium guajava* extract and its antibacterial and antioxidant properties. Asian Pac. J. Trop. Med. **7**(12), 968–976 (2014)
27. Pattanayak, M.; Nayak, P.L.: Green synthesis and characterization of zero valent iron nanoparticles from the leaf extract of *Azadirachta indica* (Neem). J. Nano Sci. Technol. **2**(1), 06–09 (2013)
28. Awwad, A.M.; Salem, N.M.: A green and facile approach for synthesis of magnetite nanoparticles. Nanosci. Nanotechnol. **2**(6), 208–213 (2012)
29. Hussain, I., et al.: Green synthesis of nanoparticles and its potential application. Biotechnol. Lett. **38**(4), 545–560 (2016)
30. Demirezen, D.A., et al.: Green synthesis and characterization of iron oxide nanoparticles using *Ficus carica* (common fig) dried fruit extract. J. Biosci. Bioeng. **127**(2), 241–245 (2019)
31. Viju Kumar, V.G.; Prem, A.A.: Green synthesis and characterization of iron oxide nanoparticles using *Phyllanthus niruri* extract. Orient. J. Chem. **34**(5), 2583 (2018)
32. Devi, H.S., et al.: Green synthesis of iron oxide nanoparticles using *Platanus orientalis* leaf extract for antifungal activity. Green Process. Synth. **8**(1), 38–45 (2019)
33. Al-Kalifawi, E.J.: Green synthesis of magnetite iron oxide nanoparticles by using Al-Abbas's (AS) hund fruit (*Citrus medica*) var sarcodactylis swingle extract and used in Al-'alqami river water treatment. J. Nat. Sci. Res **5**, 125–135 (2015)
34. Gao, C., et al.: Controllable fabrication of mesoporous MgO with various morphologies and their absorption performance for toxic pollutants in water. Cryst. Growth Des. **8**(10), 3785–3790 (2008)
35. Ehrampoush, M.H., et al.: Cadmium removal from aqueous solution by green synthesis iron oxide nanoparticles with tangerine peel extract. J. Environ. Health Sci. Eng. **13**(1), 1–7 (2015)
36. Baliga, M.S.; Kurian, P.J.: *Ixora coccinea* Linn.: traditional uses, phytochemistry and pharmacology. Chin. J. Integr. Med. **18**(1), 72–79 (2012)
37. Manuja, A., et al.: Microwave assisted fast fabrication of zinc/iron oxides based polymeric nanocomposites and evaluation on equine fibroblasts. Int. J. Biol. Macromol. **165**, 71–81 (2020)
38. Konwar, A., et al.: Chitosan–iron oxide coated graphene oxide nanocomposite hydrogel: a robust and soft antimicrobial biofilm. ACS Appl. Mater. Interfaces **8**(32), 20625–20634 (2016)
39. Ali, I., et al.: Preparation of a carboxymethylcellulose-iron composite for uptake of atorvastatin in water. Int. J. Biol. Macromol. **132**, 244–253 (2019)
40. Ali, I., et al.: Removal of copper (II) and zinc (II) ions in water on a newly synthesized polyhydroquinone/graphene nanocomposite material: kinetics, thermodynamics and mechanism. ChemistrySelect **4**(43), 12708–12718 (2019)
41. Zhao, X., et al.: Polymer-supported nanocomposites for environmental application: a review. Chem. Eng. J. **170**(2–3), 381–394 (2011)
42. Zhang, L., et al.: Synthesis of titanium cross-linked chitosan composite for efficient adsorption and detoxification of hexavalent chromium from water. J. Mater. Chem. A **3**(1), 331–340 (2015)
43. Islam, M.N., et al.: Preparation of bio-inspired trimethoxysilyl group terminated poly (1-vinylimidazole)-modified-chitosan composite for adsorption of chromium (VI) ions. J. Hazard. Mater. **379**, 120792 (2019)
44. Monteiro, O.A., Jr.; Airoldi, C.: Some studies of crosslinking chitosan–glutaraldehyde interaction in a homogeneous system. Int. J. Biol. Macromol. **26**(2–3), 119–128 (1999)
45. Li, L., et al.: Adsorbent for chromium removal based on graphene oxide functionalized with magnetic cyclodextrin–chitosan. Colloids Surf. B Biointerfaces **107**, 76–83 (2013)
46. Liu, C.; Bai, R.E.: Recent advances in chitosan and its derivatives as adsorbents for removal of pollutants from water and wastewater. Curr. Opin. Chem. Eng. **4**, 62–70 (2014)
47. Aumeeruddy, M.Z.; Zengin, G.; Mahomoodally, M.F.: A review of the traditional and modern uses of *Salvadora persica* L. (Miswak): toothbrush tree of Prophet Muhammad. J. Ethnopharmacol. **213**, 409–444 (2018)
48. Prasad, K.S.; Gandhi, P.; Selvaraj, K.: Synthesis of green nano iron particles (GnIP) and their application in adsorptive removal of As (III) and As (V) from aqueous solution. Appl. Surf. Sci. **317**, 1052–1059 (2014)
49. Anjum, M., et al.: Remediation of wastewater using various nanomaterials. Arab. J. Chem. **12**(8), 4897–4919 (2019)

50. Iravani, S.: Green synthesis of metal nanoparticles using plants. Green Chem. **13**(10), 2638–2650 (2011)
51. Kanagasubbulakshmi, S.; Kadirvelu, K.: Green synthesis of iron oxide nanoparticles using *Lagenaria siceraria* and evaluation of its antimicrobial activity. Def. Life Sci. J. **2**(4), 422–427 (2017)
52. Kaushik, A., et al.: Iron oxide-chitosan nanobiocomposite for urea sensor. Sens. Actuators B Chem. **138**(2), 572–580 (2009)
53. Brahman, K.D., et al.: Simultaneously removal of inorganic arsenic species from stored rainwater in arsenic endemic area by leaves of *Tecomella undulata*: a multivariate study. Environ. Sci. Pollut. Res. **23**(15), 15149–15163 (2016)
54. Ali, S., et al.: Synthesis, characterization, and relaxometry studies of hydrophilic and hydrophobic superparamagnetic Fe_3O_4 nanoparticles for oil reservoir applications. Colloids Surf., A **543**, 133–143 (2018)
55. Yadav, J., et al.: Characterization and antibacterial activity of synthesized silver and iron nanoparticles using *Aloe vera*. J. Nanomed. Nanotechnol. **7**(384), 2 (2016)
56. Islam, S.; Arnold, L.; Padhye, R.: Comparison and characterisation of regenerated chitosan from 1-butyl-3-methylimidazolium chloride and chitosan from crab shells. BioMed Res. Int. **2015**, 1–6 (2015)
57. Zhang, P., et al.: RETRACTED ARTICLE: Suppressor capacity of copper nanoparticles biosynthesized using *Crocus sativus* L. leaf aqueous extract on methadone-induced cell death in adrenal phaeochromocytoma (PC12) cell line. Sci. Rep. **10**(1), 1–15 (2020)
58. Hwang, S., et al.: Synthesis and characterization of iron oxide nanoparticles for phenyl hydrazine sensor applications. Sens. Lett. **12**(1), 97–101 (2014)
59. Fan, L., et al.: Preparation of magnetic modified chitosan and adsorption of Zn2+ from aqueous solutions. Colloids Surf. B **88**(2), 574–581 (2011)
60. Yuwei, C.; Jianlong, W.: Preparation and characterization of magnetic chitosan nanoparticles and its application for Cu (II) removal. Chem. Eng. J. **168**(1), 286–292 (2011)
61. Sulaiman, G.M.; Tawfeeq, A.T.; Naji, A.S.: Biosynthesis, characterization of magnetic iron oxide nanoparticles and evaluations of the cytotoxicity and DNA damage of human breast carcinoma cell lines. Artif. Cells Nanomed. Biotechnol. **46**(6), 1215–1229 (2018)
62. Akhtar, K., et al.: Novel fluoride selective voltammetric sensing method by amino phenylboronic acid-zirconium oxide nanoparticles modified gold electrode. Microchem. J. **174**, 107073 (2022)
63. Sampath, M., et al.: Green synthesis of novel jasmine bud-shaped copper nanoparticles. J. Nanotechnol. **2014**, 1–7 (2014)
64. Darwish, M.S., et al.: Synthesis of magnetic ferrite nanoparticles with high hyperthermia performance via a controlled co-precipitation method. Nanomaterials **9**(8), 1176 (2019)
65. El-Naggar, N.E.-A.; Hussein, M.H.; El-Sawah, A.A.: Phycobiliprotein-mediated synthesis of biogenic silver nanoparticles, characterization, in vitro and in vivo assessment of anticancer activities. Sci. Rep. **8**(1), 1–20 (2018)
66. Shalaby, T.I., et al.: Preparation and characterization of iron oxide nanoparticles coated with chitosan for removal of Cd (II) and Cr (VI) from aqueous solution. Water Sci. Technol. **70**(6), 1004–1010 (2014)
67. Kumar, M., et al.: Valorization of coal fired-fly ash for potential heavy metal removal from the single and multi-contaminated system. Heliyon **5**(10), e02562 (2019)
68. Aksu, Z.; Dönmez, G.: A comparative study on the biosorption characteristics of some yeasts for Remazol Blue reactive dye. Chemosphere **50**(8), 1075–1083 (2003)
69. Baek, M.-H., et al.: Removal of Malachite Green from aqueous solution using degreased coffee bean. J. Hazard. Mater. **176**(1–3), 820–828 (2010)
70. Heidari, A.; Younesi, H.; Mehraban, Z.: Removal of Ni (II), Cd (II), and Pb (II) from a ternary aqueous solution by amino functionalized mesoporous and nano mesoporous silica. Chem. Eng. J. **153**(1–3), 70–79 (2009)
71. Desta, M.B.: Batch sorption experiments: Langmuir and Freundlich isotherm studies for the adsorption of textile metal ions onto teff straw (*Eragrostis tef*) agricultural waste. J. Thermodyn. **2013**, 1–6 (2013)
72. Pandey, P., et al. Batch adsorption studies for the removal of Cu (II) ions by zeoliteNaX from aqueous stream. In: *Proceedings of the World Congress on Engineering and Computer Science, I, San Francisco, USA* (2009)
73. Gulipalli, C.S.; Prasad, B.; Wasewar, K.L.: Batch study, equilibrium and kinetics of adsorption of selenium using rice husk ash (RHA). J. Eng. Sci. Technol. **6**(5), 586–605 (2011)
74. Kundu, S.; Gupta, A.: Adsorptive removal of As (III) from aqueous solution using iron oxide coated cement (IOCC): evaluation of kinetic, equilibrium and thermodynamic models. Sep. Purif. Technol. **51**(2), 165–172 (2006)
75. Namasivayam, C.; Sureshkumar, M.: Removal of chromium (VI) from water and wastewater using surfactant modified coconut coir pith as a biosorbent. Biores. Technol. **99**(7), 2218–2225 (2008)
76. Saravanakumar, R.; Muthukumaran, K.; Selvaraju, N.: Enhanced Pb (II) ions removal by using magnetic NiO/Biochar composite. Mater. Res. Express **6**(10), 105504 (2019)
77. Lapo, B., et al.: Sorption of Hg (II) and Pb (II) ions on chitosan-iron (III) from aqueous solutions: Single and binary systems. Polymers **10**(4), 367 (2018)
78. Cheraghipour, E.; Pakshir, M.: Process optimization and modeling of Pb (II) ions adsorption on chitosan-conjugated magnetite nanobiocomposite using response surface methodology. Chemosphere **260**, 127560 (2020)
79. Abadeh, Z.A.; Irannajad, M.: Removal of Ni and Cd ions from aqueous solution using iron dust-zeolite composite: analysis by thermodynamic, kinetic and isotherm studies. Chem. Res. Chin. Univ. **33**(2), 318–326 (2017)
80. Suguna, M., et al.: Removal of Pb (II) from aqueous solutions by using chitosan coated zero valent iron nanoparticles. Sep. Sci. Technol. **49**(10), 1613–1622 (2014)
81. Ahmadi, M., et al.: Synthesis of chitosan zero-valent iron nanoparticles-supported for cadmium removal: characterization, optimization and modeling approach. J. Water Supply Res. Technol. Aqua **66**(2), 116–130 (2017)